Malaysian Journal of Chemistry, 2025, Vol. 27(2), 174-183

Enhanced Photocatalytic Performance of TiO_2/g-C_3N_4/Pt *via* In Situ Synthesis for Visible Light-Driven

Rahil Azhar[1], Nur Syamimi Adzis[1], Nur Hidayatul Syazwani Suhaimi[1], Mohd Azlan Mohd Ishak[1], Pham Trung Kien[2], Mohammad Saifulddin Mohd Azami[1], Uwaisulqarni M. Osman[3] and Wan Izhan Nawawi Wan Ismail[1]*
[1]Faculty of Applied Science, Universiti Teknologi MARA, 02600, Arau, Perlis, Malaysia
[2]Ho Chi Minh University of Technology (HCMUT), Vietnam National University, Ho Chi Minh City, Vietnam
[3]Faculty of Science and Marine Environment, Universiti Malaysia Terengganu, 21030 Kuala Nerus, Terengganu, Malaysia
*Corresponding author (e-mail: wi_nawawi@uitm.edu.my)

The increasing demand for efficient photocatalysts in environmental remediation and renewable energy has led to the exploration of advanced materials. This study focused on developing an efficient TiO_2/g-C_3N_4/Pt photocatalyst through in situ synthesis for enhanced photocatalytic performance. Characterization techniques including XRD and FTIR confirmed the presence and combination of TiO_2 and g-C_3N_4. FESEM analysis revealed a well-dispersed distribution of Pt nanoparticles on the surface of TiO_2/g-C_3N_4/Pt. The TiO_2/g-C_3N_4/Pt photocatalyst demonstrated excellent diffuse reflectance spectra (DRS) performance attributed to the surface plasmon resonance (SPR) of Pt particles which extended its absorption range into the visible light spectrum. Photoluminescence (PL) studies indicated a reduction in electron-hole recombination, particularly in the in situsynthesized samples. In the photocatalytic experiment, results showed that TiO_2/g-C_3N_4/Pt (1%) of the in situ method displayed a higher photocatalytic activity than TiO_2 and g-C_3N_4 as individual photocatalysts for the degradation of reactive red 4 (RR4) dye over 20 min. These findings indicate that the synthesis of Pt with TiO_2/g-C_3N_4 using the in situ method has significantly improved the overall optical, chemical, and physical properties of the photocatalyst.

Keywords: Reactive red 4 dye; platinum; environmental remediation; electron-hole recombination; light-driven catalysis

Received: December 2024; Accepted: February 2025

Photocatalysis has gained significant attention due to its ability to enhance wastewater remediation. Titanium dioxide (TiO_2) is an excellent and widely used semiconductor photocatalyst for photocatalytic degradation of organic pollutants in wastewater [1]. TiO_2 has unique characteristics such as photostability, low toxicity, high photocatalytic activity, low cost, and abundant availability. Despite its numerous unique features, TiO_2 has a limitation in environmental pollutant degradation due to the wide band gap energy at 3.10 eV [2, 3]. The wide band gap energy can cause limited solar spectrum utilization since photocatalytic activity efficiency is excellent under UV light [4]. Hence, nonmetal and metal doping, cocatalyst loading, coupling with visible light-responsive semiconductors, and constructing heterojunctions have been developed to address this problem.

Among them, coupling narrow band gap semiconductors with wide band gap TiO_2 appears to be a promising design to improve visible light harvesting and photoinduced charge separation [5, 6]. Graphitic carbon nitride (g-C_3N_4) has received significant attention as a visible light photocatalyst due to its low band gap, chemical stability, and excellent optical and electronic properties. This makes g-C_3N_4 a potential candidate to serve as a co-catalyst with TiO_2. However, due to the electron coupling effect, the electron-hole pairs generated by g-C_3N_4 under light excitation are easily recombined, limiting the catalytic activity and efficiency of the materials [7].

Precious metal particles such as noble metals, which Pt is part of, have been synthesized and used in organic detection and degradation fields because of their unique physical-optical properties [8–10]. Based on the Dou et al. [11], it was found that the construction of TiO_2/g-C_3N_4 modified with Pt further improves photocatalytic performance. To address the weak visible light response of TiO_2/g-C_3N_4, the introduction of Pt to form the TiO_2/g-C_3N_4/Pt composite has been proposed as an effective strategy. This approach extends the photoresponse of TiO_2/g-C_3N_4 into the visible light region through the SPR effect of Pt. In the composite, the Pt can also serve as a bridge for electron transfer. Several research has been conducted on Pt modifications such as Pt-g-C_3N_4/Bi_2WO_6 [12], 3DOM-WO_3/Pt [13], SnO_2/Pt/ln_2O_3

[14], CdS/(Pt/g-C_3N_4) [15], and Cu_2ZnSnS_4/Pt/g-C_3N_4 [16], all of which exhibited excellent photocatalytic performance.

With the advantages of incorporating noble metal nanoparticles, TiO_2/g-C_3N_4/Pt is expected to exhibit superior performance driven by improved charge carrier separation and increased efficiency. This study employed TiO_2 and g-C_3N_4 via the hydrothermal method, facilitating the in situ synthesis of TiO_2/g-C_3N_4. Pt was subsequently introduced into the composite by photodeposition, resulting in enhanced electron-hole separation efficiency and excellent photocatalytic activity under visible light. Previous studies primarily employed the batchwise method where Pt is incorporated separately after the combination of TiO_2 and g-C_3N_4. However, the batchwise method shows minimal enhancements due to the low incorporation of Pt on the surface of the combined photocatalyst. Hence, the introduction of Pt in the TiO_2/g-C_3N_4 via in situ synthesis shows improvements in the dispersion of Pt, as proven by Li et al. [17]. Several characterization techniques were used to study the morphology, surface chemical composition, and optical properties of TiO_2/g-C_3N_4/Pt (1%), which is deemed the best composite in this study. For comparison, TiO_2, g-C_3N_4, TiO_2/g-C_3N_4, and TiO_2/g-C_3N_4/Pt composite were all synthesized using the same technique. Their photocatalytic performances were evaluated by photocatalytically degrading RR4 under visible light irradiation.

EXPERIMENTAL

Materials

The chemicals used in this study were of analytical grade and used without further purification. Titanium (IV) butoxide ($C_{16}H_{36}O_4Ti$, 97%) was used as the precursor for synthesizing TiO_2. Urea sourced from HmbG Chemicals was used in the preparation of g-C_3N_4. Chloroplatinic acid (H_2PtCl_6) was employed as the Pt precursor for the deposition of Pt onto the TiO_2/g-C_3N_4 composite. Reactive red 4 dye, commonly known as Cibacron Brilliant Red, (color index: 18105, chemical formula: $C_{32}H_{23}ClN_8Na_4O_{14}S_4$, molecular weight: 995.23 g mol^{-1}, λ max: 517 nm) was chosen as the model pollutant for photocatalytic degradation studies.

Synthesis of TiO_2

TiO_2 was prepared using titanium(IV) butoxide (TBOT) as a precursor via the hydrothermal method. About 4.8 mL of distilled water was transferred into a 20 mL Teflon-lined autoclave. Next, approximately 11.8 mL of the TBOT precursor was added dropwise under ice bath conditions with continuous stirring for 1 h. The suspension was autoclaved at 180°C for 8 h. After cooling at room temperature, the obtained white suspension was washed thoroughly with distilled water several times and dried at 80°C for 1 h. The sample was annealed at 550°C for 2 h.

Synthesis of g-C_3N_4

Bulk g-C_3N_4 was prepared using a simple calcination method. About 15 g of urea was weighed and placed in the silica boat of the tube furnace. Then, the urea was calcined at 500°C for 30 min with a heating rate of 5°C/min to obtain urea products. The obtained bulk g-C_3N_4 was ground into powder at room temperature.

In Situ Synthesis of TiO_2/g-C_3N_4

For the in situ preparation of TiO_2/g-C_3N_4, about 0.8 g of as-prepared g-C_3N_4 was dispersed in 20 mL of a white suspension containing 11.8 mL of TBOT precursor and 4.2 mL of distilled water and then stirred continuously for 1 h. The mixed solution was maintained under ice bath conditions and then transferred to a Teflon autoclave for a hydrothermal process at 180°C for 8 h. After cooling to room temperature, the obtained yellow-white suspension was centrifuged at 60 rpm for 5 min and washed with distilled water several times to remove any undesired impurities. The product was dried at 80°C for 30 min. The dried yellow-white sample was placed in a crucible and ethanol was added to form a wet mixture, which was then calcined at 500°C in a tube muffle furnace for 2 h with a heating rate of 5°C/min. The as-prepared sample was labeled TCN, where TCN represents TiO_2/g-C_3N_4 synthesized using the in situ method.

Synthesis of TiO_2/g-C_3N_4/Pt

The prepared TiO_2/g-C_3N_4 was platinized via photodeposition method. The mixture solution consisting of distilled water, isopropyl alcohol (IPA), and chloroplatinic acid (H_2PtCl_6) (0.5%, 1.0%, 1.5%, 2.0%) in a Schlenk tube was bubbled with nitrogen gas for a few seconds. Then, 0.3 g of the prepared TCN was added to the solution. The mixture was purged with nitrogen and irradiated under a 250 W Xe lamp for 1 h. After photodeposition, the sample was washed thoroughly several times and dried at 110°C for 1 h. This prepared sample was labeled as TCNP, where TCNP refers to TiO_2/g-C_3N_4/Pt. Samples with different Pt loadings were designated as TCNP-0.5%, TCNP-1.0%, TCNP-1.5%, and TCNP-2.0%, respectively.

Characterization

Characterization of the unmodified and TiO_2/g-C_3N_4/Pt samples was evaluated using advanced instrumental analyses. The crystal structure was analyzed by an X-ray diffractometer (Bruker D8 Advance) using Cu Kα radiation (λ = 1.5406 Å). Fourier infrared spectroscopy-attenuated total reflectance (FTIR-ATR) was performed on a PerkinElmer Spectrum 100 to analyze the chemical composition. The surface morphology of the materials was observed using a field emission scanning electron microscope (FESEM) on a LEO SUPRA 50 VP Field Emission SEM. The UV-Visible spectra of the synthesized samples were recorded in the range of 200-800 nm using a Shimadzu UV-3600 UV-Visible-NIR spectrophotometer with $BaSO_4$ used as a reference for diffuse reflectance. The photoluminescence (PL) spectra were measured at an excitation wavelength of 420 nm at room temperature.

Photocatalytic Degradation Performance of RR4 Dye

The photocatalytic performance of as-prepared samples was evaluated through the degradation of RR4 dye under a 55 W UV-Visible lamp with a UV intensity of 3.77 W/m^2 and visible light intensity of 238 W/m^2. The lamp was positioned 10 cm in front of the solution as illustrated in **Figure 1**, ensuring uniform and constant light irradiation throughout the experiment. The degradation process was conducted in a glass cell containing 20 mL of 30 ppm RR4 solution and about 0.025 g of the photocatalyst. An aeration pump was employed to prevent dye solution depletion and maintain a consistent concentration. The reactor was continuously aerated with air supplied by the pump, enhancing mass transfer and preventing localized depletion. Initially, the system was kept in dark conditions with an aeration source for 15 min to allow the adsorption-desorption equilibrium of RR4 on the photocatalyst surface. Following this, the suspension was then exposed to simulated sunlight irradiation, and 3 mL of the solution was collected at 5-minute intervals over the total irradiation period of 20 minutes. The collected samples were then analyzed using a UV-Vis spectrophotometer at 517 nm with distilled water serving as the blank. The concentration of RR4 dye was determined by measuring its characteristic absorption peak at 517 nm. The percentage of dye degradation efficiency (D%) was calculated using Equation 1:

$$\mathrm{D\%} = \frac{A_{0-A}}{A_0}\; x\; 100\% \qquad (1)$$

Where, A_0 is the initial absorbance of the RR4 solution and A is the absorbance of the RR4 solution after visible light irradiation.

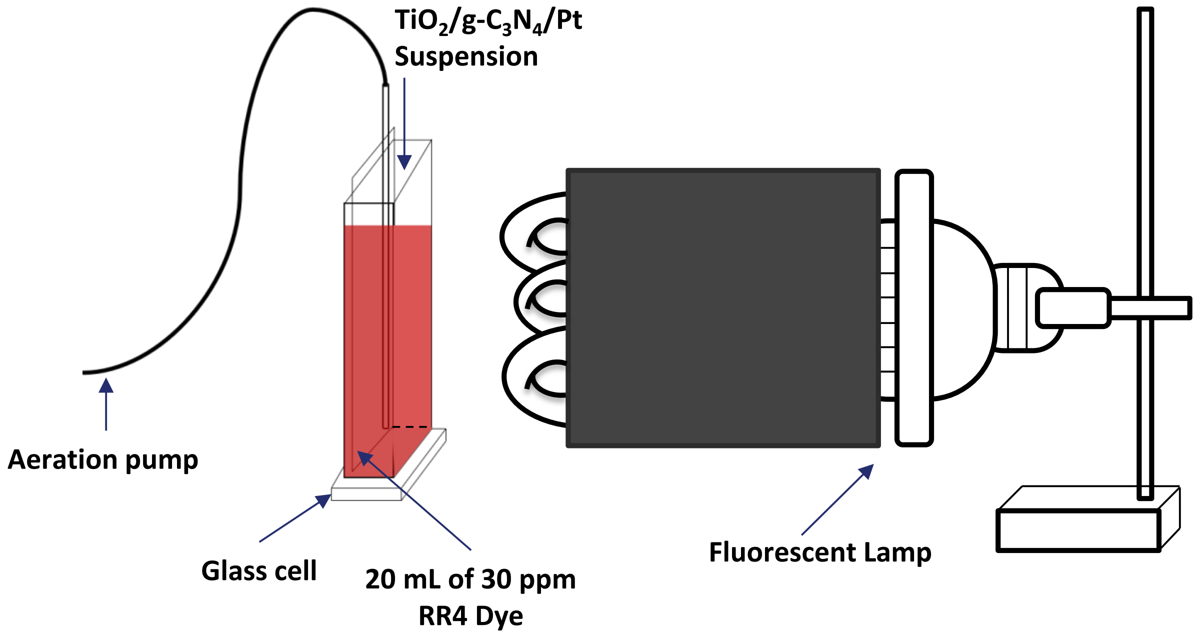

Figure 1. Experimental setup for the photodegradation process.

RESULTS AND DISCUSSION

XRD Analysis

X-ray diffraction (XRD) patterns of prepared samples for pure TiO_2, g-C_3N_4, TCN, and TCNP-1% are presented in **Figure 2(a)**. The XRD patterns of TiO_2 synthesized from the TBOT precursor via the hydrothermal method showed dominant diffraction peaks at 25.61, 38.23, 48.42, 54.26, 55.41, 63.06, 69.20, 70.58, and 75.35° assigned to (101), (004), (200), (105), (211), (213), (116), (220), and (215) crystal planes of anatase TiO_2 (JCPD No. 21–1272) [7, 16]. As previously reported [6, 17], the g-C_3N_4 sample exhibited two distinct diffraction peaks at 13.1° and 27.4°, respectively. The strong peak at 27.4° corresponds to the (002) plane, indicating the presence of interlayer stacking of aromatics structure. Meanwhile, the low intensity peak at 13.1° is associated with the (100) crystal plane of g-C_3N_4. When comparing the XRD patterns of TCN and TCNP-1%, both exhibited similar patterns to single TiO_2. The XRD spectra of TCN and TCNP-1% reveal characteristic diffraction peaks of TiO_2, confirming the co-existence of TiO_2 in the composite. Meanwhile, the characteristic diffraction peaks of g-C_3N_4 were not detected in both TCN and TCNP-1% composites. Besides, no typical diffraction peak of Pt was found in the XRD spectra of the TCNP-1% composite. This could be ascribed to the small loading of g-C_3N_4 and Pt in the as-prepared composite.

FTIR Analysis

FTIR was used to evaluate TiO_2, g-C_3N_4, TCN, and TCNP-1% with the findings presented in **Figure 2(b)**. Pure g-C_3N_4 exhibited three characteristic absorption bands around 3200 cm^{-1}, 1200-1700 cm^{-1}, and 800 cm^{-1}. The absorption band at 3200 cm^{-1} is linked to the N–H and O–H groups in the materials. The absorption peaks in the 1200-1700 cm^{-1} region correspond to the stretching vibrations of C-N heterocycles with specific peaks observed at 1640, 1573, 1413, 1318, and 1240 cm^{-1} attributed to C-N and C=N bonds [20]. Meanwhile, the weak g-C_3N_4 peaks at approximately 800 cm^{-1} are attributed to the typical plane bending mode of the tri-s-azine ring. Due to the small amount of Pt in the composite, there was no obvious difference in the FTIR spectra between TCN and TCNP-1%, showing the traces of Pt. In terms of TiO_2, the peak observed at 3328 cm^{-1} is attributed to the absorption of O–H stretching vibrations [21]. The characteristic peaks of both TiO_2 and g-C_3N_4 were observed in the TCN and TCNP-1% spectra, confirming the successful construction of the TiO_2/g-C_3N_4 composites. The presence of absorption peaks was not as intense as the pure g-C_3N_4 peak due to the low amount of g-C_3N_4 loaded into the TiO_2. This implies that the intensity of the characteristic absorbance bands of each component depends on its quantity within the composite.

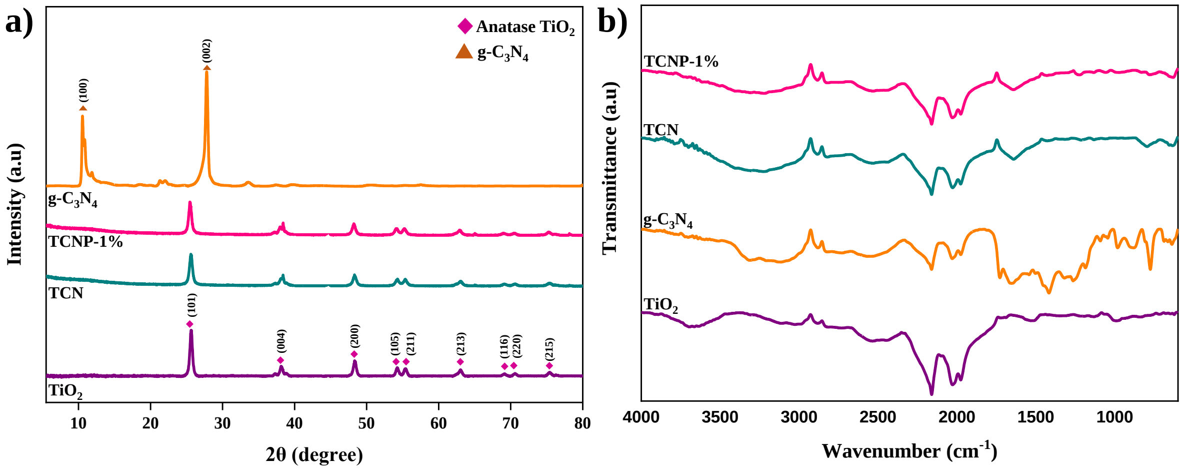

Figure 2. (a) XRD patterns of as-prepared samples: TiO_2, g-C_3N_4, TCN and TCNP-1% and (b) FTIR spectra of TiO_2, g-C_3N_4, TCN, and TCNP-1% samples.

FESEM Analysis

The morphological characteristics of TiO_2, TCN, and TCNP-1% were observed by field emission SEM and are presented in **Figure 3**. As seen in **Figure 3(a)**, the overall morphology of the TiO_2 indicates a uniform spherical morphology with a particle size about 500 nm. Upon the incorporation of g-C_3N_4 and Pt, the spherical structure on the surface of TiO_2 became less distinct, as demonstrated in the FESEM images of TCN and TCNP-1% **(Figures 3(b) & (c)).** This implies that some g-C_3N_4 and Pt may be filled with interspace of TiO_2 [22]. This result is further supported by the EDX analysis **(Figure 3(d))**, where the presence of Pt was observed and the peak of Pt appears poorly intense due to the low Pt loading introduced in the samples [23]. Element mapping was applied to distinguish the elemental distribution in the TCNP photocatalyst and the results can be seen in **Figures 3(e)-(f)**. It is clear that Pt, N, C, Ti, and O are homogeneously distributed in the composite at randomly selected areas.

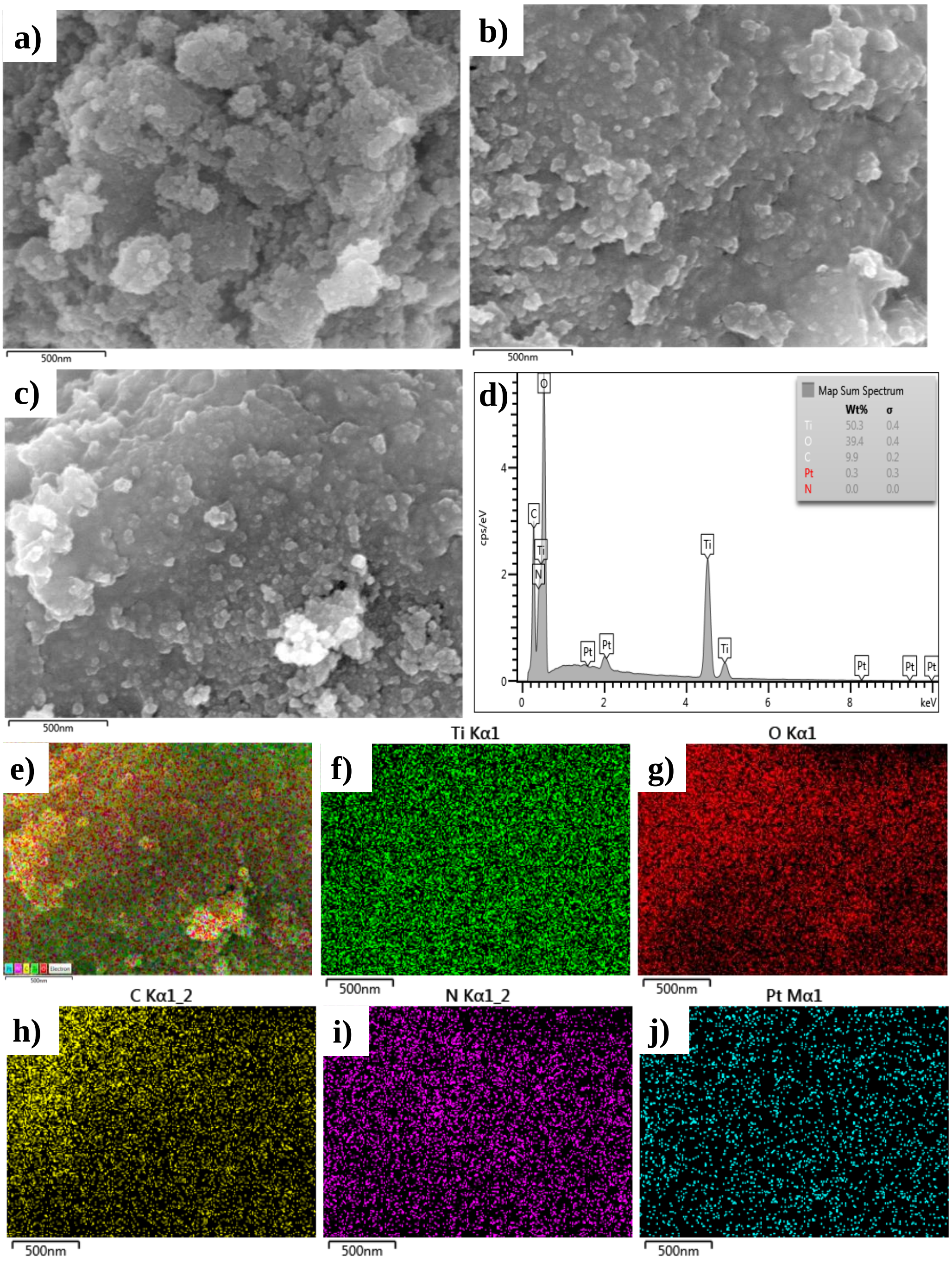

Figure 3. FESEM images of as-prepared samples of (a) pure TiO_2, (b) TCN, and (c) TCNP-1%; (d) EDX analysis; and (e)-(j) elemental mapping and elements in TCNP-1% composite.

UV-Vis DRS Analysis

The optical absorption properties of the synthesized photocatalyst were analyzed using UV-Vis DRS. In **Figure 4(a)**, pure TiO_2, with a huge band gap energy at 3.2 eV, was only active under UV light with wavelengths less than 415 nm. In contrast, pure g-C_3N_4 exhibited a broader visible light absorption range compared to TiO_2. After TiO_2 was modified with g-C_3N_4, the TCN composite showed a slight increase in its absorption range toward the visible light region. Therefore, there was less improvement in the absorption after coupling with g-C_3N_4 due to the dominant composite of TiO_2 in the ratio. Nevertheless, after the TCN composite was doped with Pt, the light absorption intensity of TCNP-1% is enhanced into the visible light range with a broadened responsive wavelength range of more than 480 nm. The results suggest that incorporating Pt significantly enhances the optical properties of the photocatalyst in the visible light region, which can be attributed to the surface plasmon resonance effect induced by Pt loading.

Furthermore, the band gap energy of the synthesized samples can be determined by using Tauc's relation, using the following Equation (2):

$$ahv = B\,(hv - E_g)^n \qquad (2)$$

Where, E_g is the band gap energy; B is the absorption constant; and n=2 for indirect transitions and n=1/2 for direct transitions. The band gaps of TiO_2, g-C_3N_4, TCN, and TCNP-1% were 3.07, 2.81, 3.05, and 2.76 eV, respectively, which correspond to their light absorption bands as shown in **Figure 4(b)**. The narrow band gap enhances the visible light absorption properties, allowing TCNP-1% to exhibit superior photocatalytic performance.

PL Analysis

PL technique is a crucial characterization to evaluate the migration, transfer, and recombination of photogenerated hole/electron pairs in photocatalysts [24]. **Figure 5(a)** presents the PL spectra of pure TiO_2, TCN, and TCNP-1% samples with an excitation wavelength of 321 nm. Pure g-C_3N_4 exhibited a strong PL emission peak around 441 nm, which is attributed to its high recombination rate of photoinduced holes and electrons. Typically, a lower PL intensity suggests reduced recombination of electron-hole pairs leading to enhanced photocatalytic activity [25]. In comparison to the TCN composite, the PL intensity of TCNP-1% was significantly decreased, indicating that Pt doping suppressed charge carrier recombination. The Pt serves as an electron mediator between TiO_2 and g-C_3N_4 in the TCNP-1% photocatalyst, allowing effective separation and migration of electron pairs in opposite directions. As a result, this improved charge separation and contributes to the higher photocatalytic activity of the TCNP-1% sample.

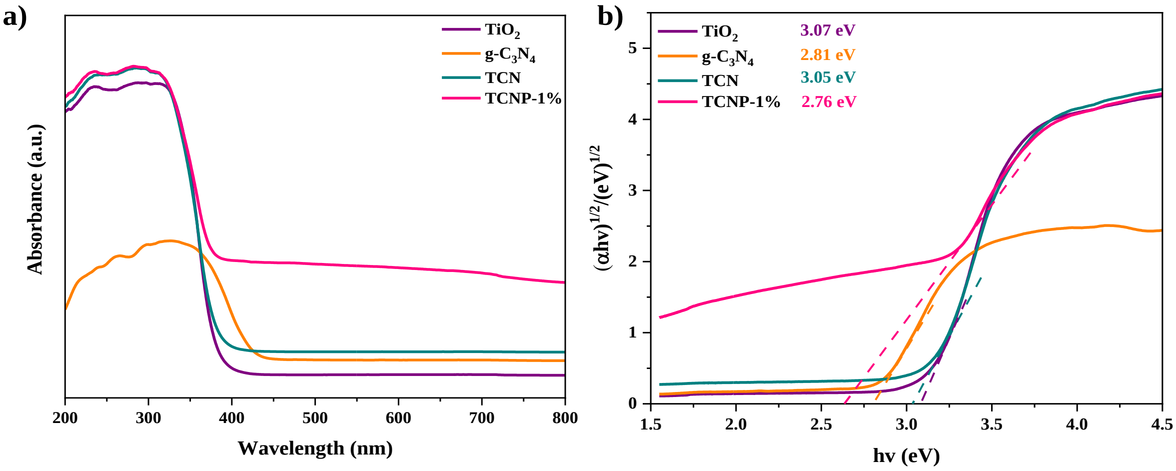

Figure 4. UV-Vis diffuse reflectance spectra (DRS) of as-prepared samples of TiO_2, g-C_3N_4, TCN, and TCNP-1% composites: (a) Absorption spectra and (b) Tauc-plot for band gap analysis.

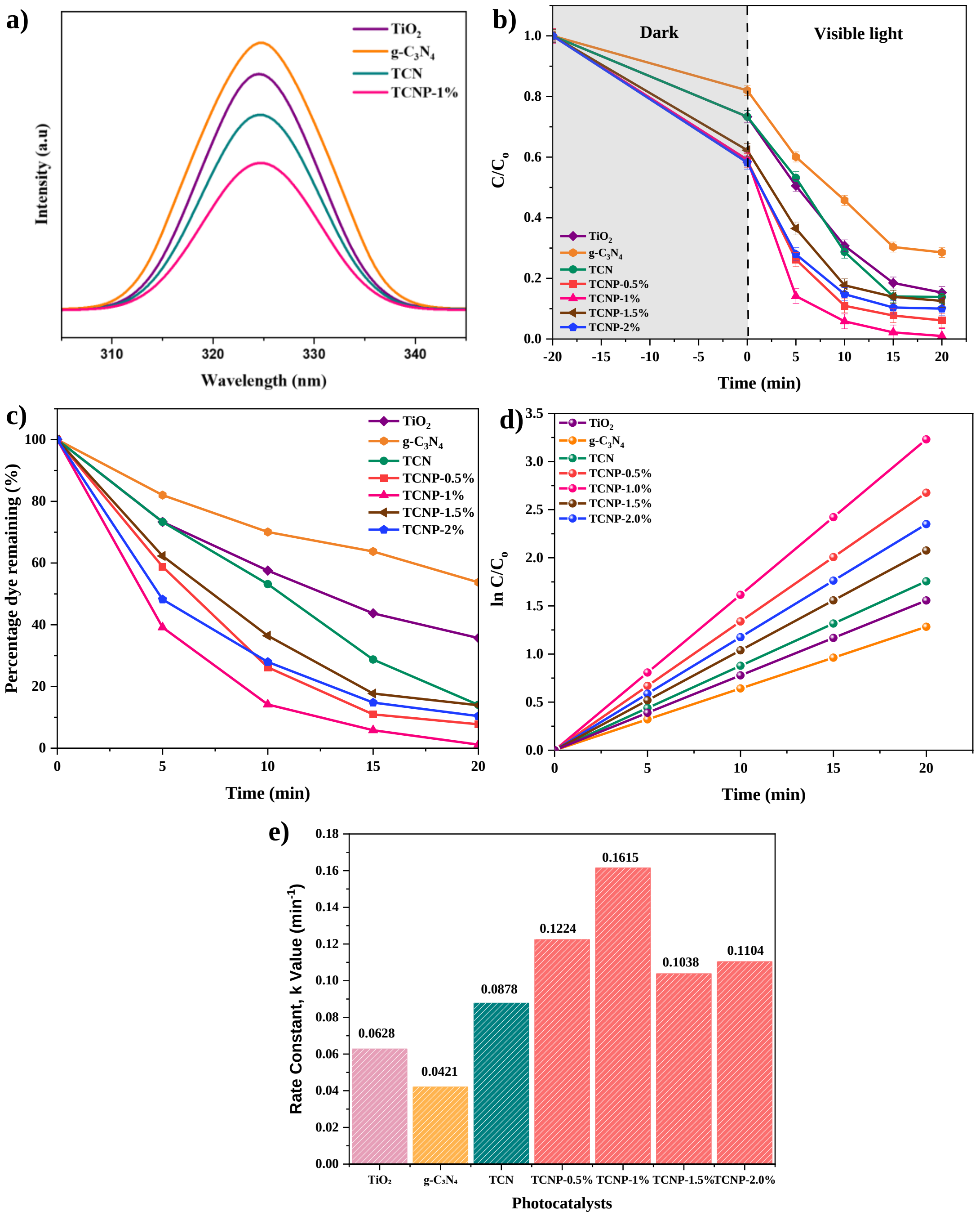

Figure 5. (a) PL spectra of pure TiO_2, g-C_3N_4, TCN, TCNP-1% samples, (b) photodegradation performance of RR4 by using different as-prepared samples under visible light irradiation, (c) the percentage of remaining dye in the degradation process of the samples, (d) first-order kinetics fitting experimental data, and (e) histogram of k values for as-prepared samples.

Photocatalytic Performance

The photocatalytic performance of the prepared samples was evaluated for the degradation of RR4 dye under visible light irradiation. The samples were subjected to an adsorption study as control study to establish adsorption-desorption equilibrium between the dye and the samples before light irradiation. Among all the samples studied, TCNP-1% exhibited a much higher photocatalytic activity, as illustrated in **Figures 5(b) & (c)**. It achieved approximately 95.83% degradation of RR4 within 20 min under visible light irradiation. In comparison, under the same conditions, the degradation rates of TiO_2, g-C_3N_4, TCN, TCNP-0.5%, TCNP-1.5%, and TCNP-2.0% were 64.29, 46.24, 85.95, 83.57, 86.08, and 89.59%, respectively. The higher photodegradation efficiency of TCNP-1% can be attributed to the fact that it possesses a stronger visible light absorption, and a higher efficiency in separation and transmission of photogenerated charge carriers than all other samples. Nevertheless, when Pt content in the TCNP photocatalyst was increased beyond the optimum level (1%), a decline in the photodegradation of RR4 was observed, owing to the excess Pt nanoparticles covering the active sites of the TCN photocatalyst. The decline in photocatalytic efficiency with higher Pt content emphasizes the necessity of optimizing Pt loading in the TCNP composite. The photocatalytic degradation kinetics was analyzed using first-order kinetics, as shown in **Figure 5(d)**, with the results plotted in the histogram of **Figure 5(e)**, following the expression in Equation (3).

$$\ln(C_0 / C) = k_{app}\, t \quad (3)$$

The variables t, C_0, and C represent the reaction time, the initial concentration of RR4 dye (mg/L), and the RR4 dye concentration at time t (mg/L), respectively. The term k_{app} denotes the pseudo-first-order rate constant (min^{-1}). Using this equation, the k values for the TiO_2, g-C_3N_4, TCN, TCNP-0.5%, TCNP-1.0%, TCNP-1.5%, and TCNP-2.0% samples were determined to be 0.0628, 0.0421, 0.0878, 0.1224, 0.1615, 0.1038, and 0.1104 min^{-1}, respectively. Notably, the TCNP-1% sample exhibited the highest k value among all samples, which was over 2 times faster than that of TCN, aligning with the photocatalytic activity trends observed in the catalyst performance curves.

CONCLUSIONS

In summary, the photocatalyst of TiO_2/g-C_3N_4/Pt was successfully prepared by an in situ hydrothermal method, which was confirmed by several characterizations. The highest photocatalytic performance for the photodegradation of RR4 dye was observed for TCNP-1%, which was about 2.6, 3.8, and 2 times larger than that of bare TiO_2, g-C_3N_4, and TCN, respectively. The enhanced photocatalytic efficiency of TiO_2/g-C_3N_4/Pt is related to the effective separation charge carriers and enhanced absorption of visible light due to the effect of Pt acting as an electron mediator and giving surface plasmon resonance effect in the composites.

Table 1. Recent reports on the preparation of TiO_2/g-C_3N_4 photocatalysts incorporated with metal doping.

Photocatalyst	Synthesis Method	Model Pollutant	Optimum	Reaction time (min)	Removal efficiency	Ref
g-C_3N_4/Ag/TiO_2	Hydrothermal (batchwise)	RhB	g-C_3N_4/Ag/TiO_2	110	< 90%	[26]
g-C_3N_4/Ag-TiO_2 hollowsphere	Simple impregnation	RhB	2%-AgTCN	105	92.7%	[27]
g-C_3N_4(Pd-Cu)/rGO/TiO_2	Hydrothermal	NO_3^- reduction	g-C_3N_4(Pd-Cu)/rGO/TiO_2	240	57.78%	[28]
PdO/g-C_3N_4/TiO_2	Impregnation	SMC	PdO/g-C_3N_4/TiO_2	-	85.6%	[29]
Hybrid 1D TiO_2/g-C_3N_4/Au	Vapor and photodeposition	H_2 evolution	HBTCN-6	-	2.22 mmol/g/h	[30]
Au/g-C_3N_4/TiO_2	Photodeposition	Rh6G	AuC-T	60	AuC-T 2 times > unmodified TiO_2	[31]
Pt/TiO_2/g-C_3N_4	Sol-gel	H_2 with sacrificial agent	3%Pt/TiO_2/g-C_3N_4	-	32.5 mmol/g/h	[32]

ACKNOWLEDGEMENT

The authors would like to express their gratitude to MARA University of Technology (UiTM) for providing the necessary facilities and support for this research. This research was funded by Geran Insentif Penyeliaan (GIP), grant no: 600-RMC/GIP 5/3 (064/2023).

The authors confirm that there are no financial conflicts of interest or personal relationships that could have influenced the work presented in this paper and the data that support the findings of this study are available upon reasonable request from the corresponding author.

REFERENCES

1. Azami, M. S., Nawawi, W. I., Jawad, A. H., Ishak, M. A. M. and Ismail, K. (2017) N-doped TiO_2 synthesised via microwave induced photocatalytic on RR4 dye removal under LED light irradiation. *Sains Malaysiana*, **46(8)**, 1309–1316.

2. Mohd Noor, N. A., Sidik, S. M., Rosmi, M. S., Che Ku Hitam, C. K. N. L. and Jaafar, N. F. (2022) Advancement of TiO_2 -based photocatalyst for photodegradation of organic pollutants in wastewater, *Central Asia and The Caucas*, **23(1)**, 2021–2049.

3. Alias, S. H., Mohamed, N. N., Loon, L. W. and Chandren, S. (2019) Synthesis of carbon self-doped titanium dioxide and its activity in the photocatalytic oxidation of styrene under visible light irradiation. *Malaysian Journal of Fundamental Applied Sciences*, **15(2)**, 291–297.

4. Ho, V. T. T., Chau, D. H., Bui, K. Q., Nguyen, N. T. T., Tran, T. K. N., Bach L. G. and Truong, S. N. (2022) A high-performing nanostructured Ir doped-TiO_2 for efficient photocatalytic degradation of gaseous toluene. *Inorganics*, **10(3)**.

5. Yuan, Y., Guo, R. T., Hong, L. F., Ji, X. Y., Lin, Z. D., Li, Z. S. and Pan, W. G. (2021) A review of metal oxide-based Z-scheme heterojunction photocatalysts : actualities and developments. *Materials Today Energy*, **21**, 100829.

6. Li, Y., Wang, G., Zhang, H., Qian, W., Li, D. and Guo, Z. (2022) Hierarchical flower-like 0D/3D g-C_3N_4/TiO_2 S-scheme heterojunction with enhanced photocatalytic activity. *Colloids Surfaces A: Physicochemical and Engineering Aspects*, **646**, 128942.

7. Qian, H., Zhou, J., Liu, H., Ma, A., Xu, S., Li, T. and Ren, S. (2024) Construction of direct-Z-scheme heterojunction photocatalyst of g-C_3N_4/Ti_3C_2/TiO_2 composite and its degradation behavior for dyes of Rhodamine B. *Chinese Journal of Chemical Engineering*, **73**, 222–234.

8. Wu, J., Chen, L., Fu, T., Zhao, H. B., Guo, D. M., Wang, X. L. and Wang, Y. Z. (2018) New application for aromatic Schiffbase: High efficient flame-retardant and anti-dripping action for polyesters. *Chemical Engineering Journal*, **336**, 622–632.

9. Qin, L., Zeng, G., Lai, C., Huang, D., Zhang, C. and Xu, P. (2017) A visual application of gold nanoparticles : Simple, reliable and sensitive detection of kanamycin based on hydrogen-bonding recognition. *Sensors Actuators B: Chemical*, **243**, 946–954.

10. Qin, L., Zhen, G., Lai, C., Huang, D., Xu, P., Zhang, C., Liu, X., Liu, S., Li, B. and Yi, H. (2018) "Gold rush" in modern science : Fabrication strategies and typical advanced applications of gold nanoparticles in sensing. *Coordination Chemistry Reviews*, **359**, 1–31.

11. Dou, H., Qin, Y., Pan, F., Long, D., Rao, X., Xu, Q. G. and Zhang, Y. (2019) Core-shell g-C_3N_4/Pt/TiO_2 nanowires for simultaneous photocatalytic H_2 evolution and RhB degradation under visible light irradiation. *Catalysis Science and Technology*, **9(18)**.

12. Qin, L., Zeng, G., Lai, C., Huang, D., Xu, P., Zhang, C., Cheng, M., Liu, X., Liu, S., Liu, B., Yi, H. (2019) Construction of Pt-decorated g-C_3N_4/Bi_2WO_6 Z-scheme composite with superior solar photocatalytic activity toward rhodamine B degradation. *Coordination Chemistry Reviews*, **100**.

13. Yan, X., Xia, M., Xu, B., Wei, J., Yang, B. and Yang, G. (2018) Fabrication of novel all-solid-state Z-scheme heterojunctions of 3DOM-WO_3/Pt coated by mono-or few-layered WS2 for efficient photocatalytic decomposition performance in Vis-NIR region. *Applied Catalysis B: Environmental*, **232**, 481–491.

14. Sun, Y., Zhu, Q., Bai, B., Li, Y. and He, C. (2020) Novel all-solid-state Z-scheme SnO_2/Pt/In_2O_3 photocatalyst with boosted photocatalytic performance on water splitting and 2, 4-dichlorophenol degradation under visible light. *Chemical Engineering Journal*, **390**, 124518.

15. Hu, W., Zhang, J., Tian, J., Dang, Y., Wang, W., Zhan, H. and Ma, B. (2022) Greatly enhanced photocatalytic hydrogen production on CdS/(Pt/g-C_3N_4) via dual functions of Pt on semiconductors interface. *International Journal of Hydrogen Energy*, **47(68)**, 29295–29304.

16. Raza, A., Shen, H. and Haidry, A. A. (2020) Novel Cu_2ZnSnS_4/Pt/g-C_3N_4 heterojunction photocatalyst

with straddling band configuration for enhanced solar to fuel conversion. *Applied Catalysis B: Environmental*, **277**, 119239.

17. Li, Q., Lu, M., Wang, W., Zhao, W., Chen, G. and Shi, H. (2019) Fabrication of 2D/2D g-C_3N_4/Au/Bi_2WO_6 Z-scheme photocatalyst with enhanced visible-light-driven photocatalytic activity. *Applied Surface Science*, **508**, 144182.

18. Zheng, L., Xiao, X., Li, Y. and Zhang, W. (2017) Enhanced photocatalytic activity of TiO_2 nanoparticles using WS_2/g-C_3N_4 hybrid as co-catalyst. *Transactions of Nonferrous Metals Society of China*, **27**.

19. Li, J., Song, W., Zhang, X. and Zhao, Z. (2020) All-solid-state Z-scheme photocatalysts of g-C_3N_4/Pt/macroporous-(TiO_2 @ carbon) for selective boosting visible-light-driven conversion of CO_2 to CH_4. *Journal of Catalysis*, **389**, 440–449.

20. Liu, N., Lu, N., Yu, H., Chen, S. and Quan, X. (2020) Efficient day-night photocatalysis performance of 2D/2D Ti_3C_2/Porous g-C_3N_4 nanolayers composite and its application in the degradation of organic pollutants. *Chemosphere*, **246**.

21. Suwarnkar, M. B., Dhabbe, R. S., Kadam, A. N. and Garadkar, K. M. (2014) Enhanced photocatalytic activity of Ag doped TiO_2 nanoparticles synthesized by a microwave assisted method. *Ceramics International*, **40(4)**, 5489–5496.

22. Zheng, L., Xiao, X., Li, Y., Zhang, W. (2017) Enhanced photocatalytic activity of TiO_2 nanoparticles using. *Transactions of Nonferrous Metals Society of China*, **27**.

23. Adzis, N. S., Suhaimi, N. H. S., Abdul Ghani, N. I., Abd Yami, N. F. N., Muhamad, N. A., Mohd Azami, M. S. and Ismail, W. I. N. (2023) Modification of Silver Oxide / Silver Doped Titanium Dioxide (Ag_2O/Ag-TiO_2) Photocatalyst Using an Immobilized Reverse Photodeposition Method for Photodegradation of Reactive. *Malaysian Journal Chemistry*, **25(4)**, 184–198.

24. Ou, M., Wan, S., Zhong, Q., Zhang, S., Song, Y., Guo, L., Cai, W. and Xu, Y. (2017) Hierarchical Z-scheme photocatalyst of g-C_3N_4@Ag/$BiVO_4$ with enhanced visible-light-induced photocatalytic oxidation performance. *Applied Catalysis B: Environmental*, **4(040)**.

25. Luo, M., Yao, W., Huang, C., Wu, Q. and Xu, Q. (2015) Shape effects of Pt nanoparticles on hydrogen production via Pt/CdS photocatalysts under visible light. *Journal of Materials Chemistry A*, **3(26)**, 13884–13891.

26. Xu, J. and Ma, S. (2023) High-efficiency photocatalytic degradation of RhB by protonation of g-C_3N_4 with Ag-loaded TiO_2 nanofibers. *Journal of Crystal Growth*, **617**, 127290.

27. Sui, G., Li, J., Du, L., Zhuang, Y., Zhang, Y., Zou, Y. and Li, B. (2020) Preparation and characterization of g-C_3N_4/Ag–TiO_2 ternary hollowsphere nanoheterojunction catalyst with high visible light photocatalytic performance. *Journal of Alloys and Compdounds*, **823**, 153851.

28. Li, H., Xue, S., Cao, F., Gao, C., Wei, Q., Li, R., Zhou, A., Wang, S. and Yue, X. (2023) Enhanced nitrate reduction by metal deposited g-C_3N_4/rGO/TiO_2 Z-schematic photocatalysts: Performance and mechanism comparison of Pd-Cu and Ag. *Chemosphere*, **325**, 138336.

29. Xu, Y., Li, Y., Wei, Y., Liang, H., Xu, T., Sun, Y. and Bai, J. (2024) Facile synthesis of Pd loaded g-C_3N_4/TiO_2 heterojunction catalyst with enhanced photothermal catalytic performance in Suzuki coupling under moderate condition. *Colloids Surfaces A: Physicochemical and Engineering Aspects*, **690**, 133751.

30. Nasir, M. S., Yang, G., Ayub, I., Wang, S. and Yan, W. (2020) In situ decoration of g-C_3N_4 quantum dots on 1D branched TiO_2 loaded with plasmonic Au nanoparticles and improved the photocatalytic hydrogen evolution activity. *Applied Surface Science*, **519**, 146208.

31. Wei, T., Xu, J., Kan, C., Zhang, L. and Zhu, X. (2022) Au tailored on g-C_3N_4/TiO_2 heterostructure for enhanced photocatalytic performance. *Journal of Alloys and Compounds*, **894**, 162338.

32. Zhang, B., Jin, X., Li, X., Dong, L., Liu, D., Zhang, Y., Zhao, Z., Ge, Q. and Zhang, F. (2024) Piezoelectric assisted boosting photocatalytic hydrogen evolution over a finely prepared Pt/TiO_2/g-C_3N_4 composite system using lactic acid as sacrificial agent. *International Journal of Hydrogen Energy*, **84**, 480–490.